

Energy-Efficient Implementation of Spiking Recurrent Cells on FPGA

Pascal Harmeling^{1,*}, Florent De Geeter¹ and Guillaume Drion¹

May 13, 2026

Abstract

Spiking Neural Networks (SNNs) can reduce energy consumption compared to conventional Artificial Neural Networks (ANNs) when spiking activity is sparse and the neuron model is hardware-friendly. However, biologically faithful models are often too costly to implement on FPGAs, whereas very simple models (e.g., IR/LIF) sacrifice part of the neuronal dynamics. In this work, we present an FPGA accelerator for an SNN using Spiking Recurrent Cell (SRC) neurons, providing a trade-off between biological plausibility and hardware cost. We propose a set of mathematical simplifications that remove costly unary operators (*tanh*, *exp*) and avoid floating-point arithmetic through scaling and piecewise-defined approximations. The complete network is implemented in VHDL and validated using spiking traces derived from the MNIST dataset. The weight matrices computed off-line are stored directly in LUT-registers without any adaptation. This demonstrates the robustness of SRC cells. Experiments were conducted on an Artix-7 XC7A200T clocked at 100 MHz. The reference implementation achieves 96.31% accuracy with a 220-image spiking trace and a processing time of 1.7424 ms per digit. We then investigate accuracy/energy trade-offs by reducing the spiking trace length and quantizing synaptic weights down to 4 bits, achieving 93.32% accuracy at 0.55 mJ per digit (55 images, 5-bit weights) and 92.89% at 0.45 mJ (44 images, 4-bit weights). These results show that SRC-based SNNs can deliver competitive performance with reduced energy consumption, while preserving richer neuronal dynamics than standard LIF/IR models.

1 Introduction

Artificial neural networks (ANNs) have undergone constant evolution over the past few decades, surpassing human performance in many areas. However, their energy consumption for learning and inference is increasing [20], which hinders their large-scale deployment in energy-constrained environments. On the other hand, biological brains only consume a few tens of watts of power to function, due to the sparse spiking nature of their computation.

Spiking neural networks (SNNs) have emerged as a low-power alternative to traditional ANNs, leveraging event-driven processing to emulate the efficiency of biological neural computations. SNNs have shown promising performance-consumption trade-offs, especially when deployed on dedicated hardware [5, 23]. However, SNN energy consumption strongly depends on spiking model complexity, as well as on spiking frequency, i.e., sparsity [2]. There exists a plethora of spiking neuron model types, ranging from simple Integrate-and-Fire (IF) models [1, 7] up to biologically-inspired conductance-based model that follows the Hodgkin–Huxley formalism [11, 19]. Although the field of neuronal modeling is in constant evolution, SNNs mostly implement leaky integrate-and-fire (LIF) models and their variants, due to their computational simplicity.

SNNs performance and power efficiency also strongly depend on the type of hardware being used. SNNs can be implemented on Central Processing Units (CPUs), similarly to classical ANNs, but these implementations bring little advantage as CPU architecture is poorly suited for sparse computations. In particular, the limited parallelism of CPU processing makes such implementations unable to deliver real-time performance for large-scale networks [21]. Application-Specific Integrated Circuits (ASICs) can overcome this limitation [16]. Full parallelization then becomes possible by tailoring the hardware architecture to the entire neural network. However, this advantage is offset by the inability to reprogram the device once it has been manufactured.

Field-Programmable Gate Arrays (FPGAs) provide a third alternative, allowing for programmable, energy-efficient implementation of a very large number of tasks in parallel. In addition, the integration of memory blocks (BRAM) and Digital Signal Processing (DSP) modules within FPGAs makes it possible to closely emulate the behavior of neural networks, while ensuring efficient learning and adaptation to the target tasks with minimal energy consumption [14]. This hardware approach, commonly referred to as an FPGA-based accelerator, constitutes a particularly relevant solution for the study of SNNs. FPGA implementations of SNNs using LIF models have emerged over the past few years (e.g., Carpegna et al. [3, 4], Gupta et al. [8], Han et al. [9], He et al. [10], Li et al. [14, 13]). LIF model simplicity allows for reduced hardware resources and computation time, but they rely on a reset mechanism that deviates from biological behavior.

In this work, we introduce an SNN FPGA implementation based on Spiking Recurrent Cell (SRC) [6]. SRC neurons are derived from classical recurrent neural network (RNN) architectures and integrate spiking behavior directly into their dynamics, eliminating the need for an explicit reset. We propose a series of simplifications of the original SRC equations to improve implementation efficiency on the FPGA, and construct a modulatory architecture aiming at general-purpose deployment.

We trained and tested the system on the MNIST dataset. To investigate the robustness properties of the SRC network, we first trained the original, unsimplified network of De Geeter et al. [6], and directly transferred the weight matrices into the simplified FPGA system without modification. We then explored the impact of weight quantization, which reduces the memory footprint at the expense of accuracy. We demonstrate that the FPGA implementation of the SRC network achieves performance comparable to leading LIF approaches in terms of accuracy and power consumption.

2 Related work

Tables 1 and 2 summarize the performance of FPGA implementations of LIF-based SNNs in terms of, e.g., computation time, energy consumption per processed MNIST image, and image recognition accuracy. Table 1 contains models with online learning rules embedded on the FPGA. Table 2 shows models for which learning is performed offline. In both cases, the image recognition rate remains high and is often above 90%.

The solutions proposed by Gupta et al. [8], Carpegna et al. [3, 4], Li et al. [13] achieve image processing times below one millisecond. In all cases, the use of LIF-type neurons enables a simpler yet efficient implementation of the neural network.

The work by Carpegna et al. [3] presents a layered architecture and an associated implementation method, achieving low resource utilization and reduced energy consumption. The study of Han et al. [9] highlights that excessive quantization of the weights W leads to a significant degradation in accuracy, suggesting the existence of a minimum word-length threshold. However, depending on the learning method, good performance can still be achieved with a 4-bit weight representation [17]. In this work, we explore a wide quantization range, from 9 down to 2 bits (including the sign bit).

Spike management and inter-layer data transfer must also be carefully designed. The *event-*

Table 1. Comparison of FPGA-based SNN implementations (MNIST) - On-chip learning.

Design	Li et al. [14]	Gupta et al. [8]	He et al. [10]
Year	2021	2020	2021
Model	LIF	LIF	LIF
Neurons	784-200-100-10	784-16	784-2048-100
FPGA	VIRTEX-7	XC6VLX240T	Zynq7045
<i>freq.</i> [MHz]	100	100	100 (200) ¹
Cells log.	-	79,468	23180
DSP used	-	64	8
BRAM used	-	16	129
Weight (bits)	16	24	
<i>T/ing</i> [ms]	3.15	0.5	66.6 (33.3) ¹
<i>E/ing</i> [mJ]	5.04	-	
Accuracy [%]	92.93	-	93.00

¹ Initial values tested at 200 MHz

driven approach proposed by Roy et al. [18] is highly efficient when spikes are sparse, but becomes less effective under dense or bursty activity. In such cases, synchronous layer-by-layer processing [22] is commonly adopted. Here, we employ a synchronous per-layer processing scheme, leveraging the parallelism offered by the FPGA.

3 Adaptation of SRC equations for efficient FPGA implementation

In our implementation, we use the SRC model in the intermediate layer to preserve continuous neuronal dynamics while remaining compatible with efficient hardware simplification. We first describe original SRC equations and then propose a set of mathematical simplifications that allow for efficient FPGA implementation.

3.1 Original SRC equations

The SRC equations are written as

$$\begin{cases} h[t] = \tanh(I[t] + r \cdot h[t-1] + r_s \cdot h_s[t-1] + b_h), \\ h_s[t] = z_s[t] \cdot h_s[t-1] + (1 - z_s[t]) \cdot h[t-1], \\ z_s[t] = z_s^{hyp} - (z_s^{hyp} - z_s^{deep}) \frac{1}{1 + \exp(-10(h[t-1] - 0.5))}, \end{cases} \quad (1)$$

where $I[t]$ represents the current input to the system and $h[t]$ corresponds to its output (the spike-generation equation). The equation for $h_s[t]$ introduces refractory-type dynamics whose relaxation time is defined by $z_s[t]$. Higher values of $z_s[t] < 1$ lead to slower relaxation, hence lower firing frequencies. The parameters r , r_s , b_h , z_s^{hyp} , and z_s^{deep} are fixed and depend on the implementation method and the desired sensitivity. The values used by De Geeter et al. [6] are respectively $r = 2$, $r_s = -7$, $b_h = -6$, $z_s^{hyp} = 0.9$, and $z_s^{deep} = 0.0$.

Table 2. Comparison of FPGA-based SNN implementations (MNIST) - Offline learning.

Design	Carpegna et al. [3]	Carpegna et al. [4]	Han et al. [9]	Li et al. [13]
Year	2022	2024	2020	2023
Model	LIF	LIF	LIF	IF/LIF
Neurons	1384	784-128-10	784-1024-1024-10	784-16C3-...-10 ¹
FPGA	ARTIX-7	XC7Z020	XC7Z045 SoC	XCZU3eg
<i>freq.</i> [MHz]	100	100	100 ²	300
Cells log.	-	7,612	12,690	-
DSP used	-	0	-	-
BRAM used	45	18	40.5	-
Weight (bits)	5	4	16	-
<i>T/img</i> [ms]	0.215	0.78	12.42 ²	0.491
<i>E/img</i> [mJ]	13	0.14	5.92 ²	1.25
FPGA accur[%]	73.96	93.85	97.06	98.12

¹ 784-16c3-64c3-p2-128c3-p2-256c3-256c3-10² adjust from 150 to 100 MHz

This study primarily focuses on the benefits of a hardware implementation on an FPGA. The learning process is deliberately only briefly addressed, since the parameters (bias b_h and weights $w_{i,j}$) are directly taken from the network implemented in Julia. No transformation is required, which represents a significant advantage when porting the design to the VHDL language.

3.2 Simplified SRC equations

A key step in the FPGA implementation is the simplification of the SRC neuron equations while preserving their dynamics. Unary operators such as *tanh* and *exp*, as well as the use of floating-point number representations, are hardware-expensive and often highly energy-consuming.

The first simplification consists in eliminating floating-point arithmetic. To achieve this, all variables and parameters are scaled by a factor 1000 and converted into integer values. This provides sufficient precision while limiting the register size to 11 bits (numerical representation from -1024 to $+1023$). Secondly, the unary operator *tanh* is replaced by a piecewise-defined function (*Stanh*) to simplify the number of operations to be implemented (Figure 1). A slope of 0.75 is selected in order to minimize the approximation error. Third, the operation $y = (3x)/4$ is implemented in VHDL as $y = (2x + x)/4$ using shift operations:

$$y = \text{shiftright}((\text{shiftleft}(x, 1) + x), 2) \quad (2)$$

The operator *exp*() used in $z_s[t]$ cannot be easily simplified, and its use within a fraction further increases the complexity. However, one can observe that $z_s[t]$ acts as a switching mechanism between a slow and a fast dynamical regime, as shown in Figure 2. In practice, the values of z_s remain close to either z_s^{deep} or z_s^{hyp} . By determining a switching threshold, the function determining $z_s[t]$ can be replaced by a simple threshold rule: if $h[t - 1]$ is greater than $V_{th}(z)$, then $z_s[t] = z_s^{deep}$; otherwise, $z_s[t] = z_s^{hyp}$. This operation can be implemented in VHDL using a *if* statement.

Finally, the parameter r_s is adjusted from -7 to -8 . This modification yields even-valued parameters, enabling multiplications to be implemented using shift operations, without affecting

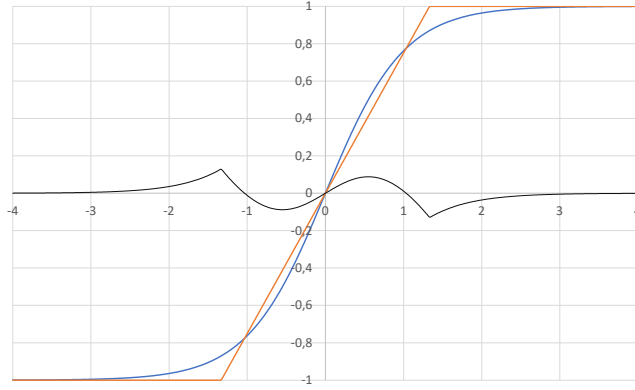


Figure 1. Simplification of the \tanh function using Stanh .
Tanh() - Stanh() - Error

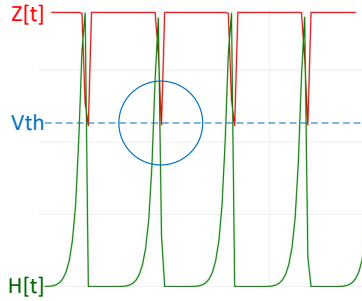


Figure 2. Simplification of the function $z[t]$ into a threshold rule with detection threshold $V_{th}(z)$

model dynamics. This also makes it possible to remove the explicit parameters r and r_s and to adjust b_h (which becomes 3000 after scaling). Likewise, factoring out $z_s[t]$ allows us to merge two multiplications into a single operation. The simplified SRC equations are written as

$$\begin{cases} \text{Work} = I[t] + (h[t - 1] - (h_s[t - 1] \lll 2) + b_h) \lll 1, \\ h[t] = \text{Stanh}(((\text{Work} \lll 1) + \text{Work}) \ggg 2), \\ h_s[t] = ((z_s[t] \cdot (h_s[t - 1] - h[t - 1])) \ggg 10 + h[t - 1]), \\ z_s[t] : \text{if}(h[t] < 500) \rightarrow z_s^{\text{hyp}} \text{ else } \rightarrow z_s^{\text{deep}}, \end{cases} \quad (3)$$

where Work serves as an intermediate variable.

We next investigate the impact of these simplifications on model dynamics by comparing the outputs of the two different SRC implementations. The first SRC is implemented in Julia using a `FLOAT32` representation and does not undergo any simplification. The second SRC uses only an `INT16` representation together with all the simplifications proposed above. This second version is referred to as Pseudo-VHDL (PsV). During this evaluation step, z_s^{hyp} and z_s^{deep} are initialized to 0.910 and 0.000 in the original implementation, and to 902 and 100 in the PsV implementation. The values 902 and 100 are selected to best approximate the frequency behavior reported by De Geeter et al. [6]. Figure 3 illustrates the behavior of the output $h[t]$ when implemented in Julia (green) and

in PsV (red), showing a very good match between the two versions.

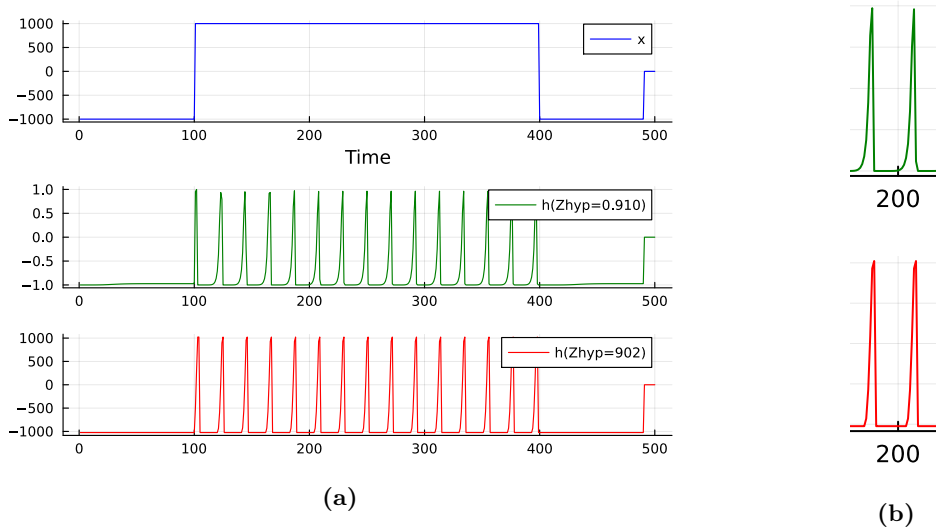


Figure 3. (a) Behavior of the output $h[t]$ as a function of the implementation, Julia and PsV, (b) with a zoomed comparison of spikes generated in Julia and PsV.

Inferences of the complete PsV network implementation are first carried out in Julia in order to compare the original SRC network with our simplified version. To ensure a fair comparison, it is essential to use exactly the same Spiking Trace (SpT) sequences. A spiking trace is a sequence of binary images (0/1) intended to simulate a stream of spikes at the input. This set is constructed from a single MNIST sample. All elements of the MNIST test set are processed by a Julia code following the procedure illustrated in Figure 4. The first step consists in discretizing an MNIST image into binary values (0/1): pixels with values greater than 0.5 are set to 1, otherwise to 0. This binary image is then used to generate a sequence of 200 images using a Bernoulli process with a maximum probability of 0.25. A filtering step prevents a given pixel from remaining at 1 in two consecutive images. Finally, 20 all-black images are added at the beginning, serving as a reset window as done by De Geeter et al. [6]. The resulting sequence of 220 images constitutes a spiking trace. This processing is applied to all 10,000 images of the MNIST test set and saved into 10,000 NPY files. Over the entire test set, the original implementation achieves an accuracy of 96.48%, while the PsV implementation reaches 96.31%.

To test performance stability with respect to spike frequency, a second series of tests is performed by modifying the value of the parameter z_s^{hyp} . Figure 5a shows spiking frequency as a function of z_s^{hyp} . Approximately three times fewer spikes are observed when z_s^{hyp} increases from 880 to 980. For this test, z_s^{deep} is fixed to 0.000 in the original implementation and to 100 in the PsV implementation.

Figure 5b shows the accuracy of both models as a function of z_s^{hyp} . Both models show a high and stable accuracy for a large range of parameter values. This shows that it is possible to reduce the spike generation rate at the output of the SRC neurons without significantly affecting accuracy, thereby enabling a reduction in energy consumption through increased spike sparsity. The range $z_s^{hyp} \in [880, 980]$ will later be used to evaluate the stability and accuracy of the SRC network when implemented in VHDL and executed on an FPGA.

Finally, we compare the dynamics of IR outputs in both implementations (Figure 8). In most

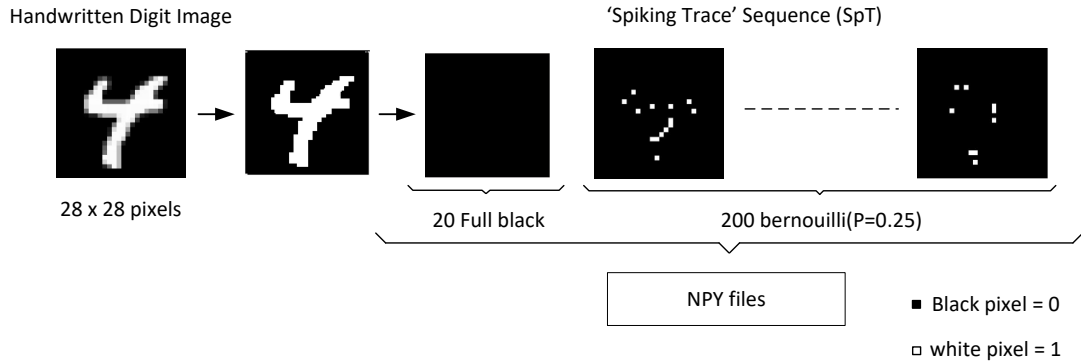


Figure 4. MNIST dataset processed by a Julia code, spiking traces.

cases, both models show very similar output dynamics, the only difference occurs when the classification decision is unclear (Figure 9).

4 Implementation architecture

The architecture presented in this work is a layered system, similar to that described in the work of Carpegna et al. [3]. Our network is composed of four layers: the input interface (`Neuron_BramInLine_pkg`), the SRC neuron layer (`Neuron_Src2F_pkg`), the IR integrator neuron layer (`Neuron_LIfB_pkg`), and finally a comparator that outputs a value between 0 and 9 (`Neuron_Cmp_pkg`). Figure 6 presents the detailed construction of the architecture.

In order to obtain an efficient network, all neurons are processed in parallel using the `GENERATE` operator in VHDL. Since each layer may have a different computation time, synchronization of data transfers between layers is essential. This synchronization is handled by the main module, referred to as the *Binder*. The *Go*, *Ready*, and *Latch* signals ensure synchronization across the different levels. All processes share the same clock (100 MHz) and the same *reset* signal. The *Binder* also routes signals and spike vectors between the different levels.

Figure 7 shows the internal structure of each “`NetWorkLevelxx.vhd`” module. They contain a weight matrix encoded in a file named “`WeightMatrixx.vhd`”, as well as the code associated with the neuron type used in that layer. To facilitate the layered construction of the network, `NetWorkLevel` module structures are identical and each module only differ in its internal neuron package.

4.1 Input interface

The input layer provides the SRC layer with a vector representing one image from a SpT sequence. Each image is composed of 28×28 pixels, yielding a vector size of 784 bits. The FPGA board used is an Alinx AX7A200B equipped with an AMD Xilinx Artix-7 XC7A200T shown in Figure 10. It includes internal BRAM memory in which the spiking traces are stored. The NPY files are converted into COE files compatible with Vivado. During this conversion, six additional bits are appended to each image: two bits dedicated to a micro-machine (μ -*RESET* and μ -*CMP*) and four bits containing the target digit *CMP_VAL*. These six bits can be considered as neuromodulatory signals. The μ -*RESET* signal is activated at the beginning of each spiking trace to reset the neurons, while μ -*CMP*

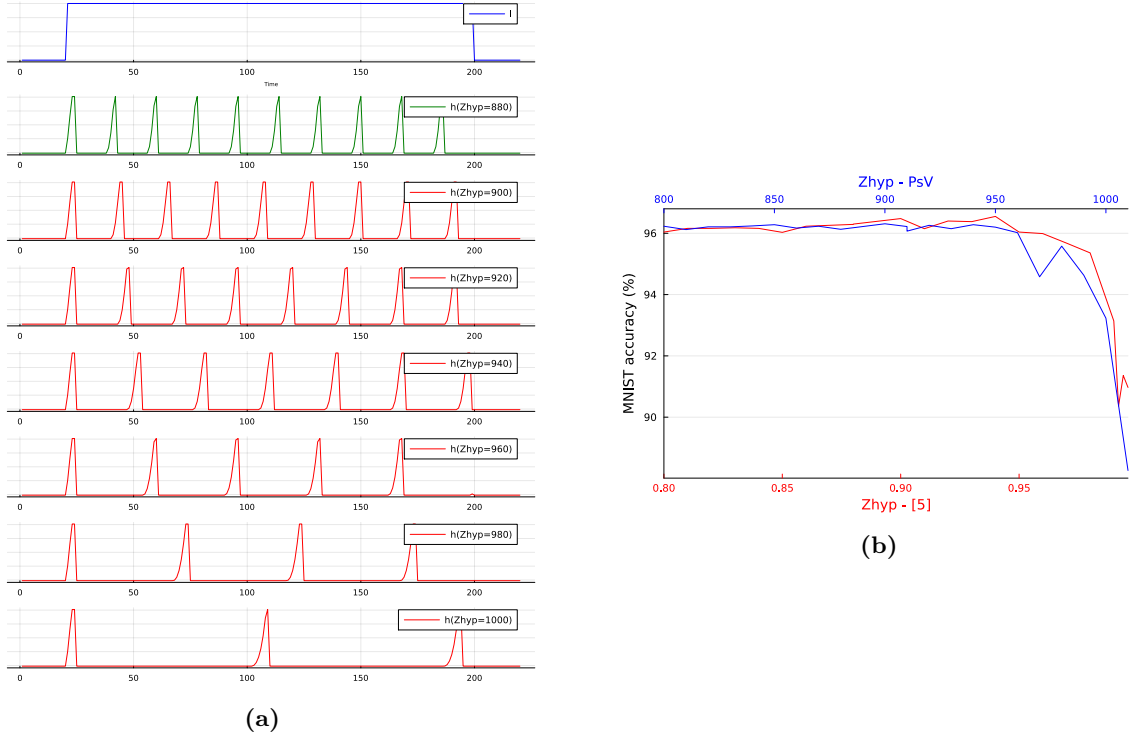


Figure 5. (a) Spike generation frequency at the output of h_s as a function of the value of z_s^{hyp} . (b) Stability results and accuracy

is activated at the end of the trace to enable the comparison between the discriminator output and *CMP_VAL*.

4.2 SRC layer and IR layer

The SRC layer receives an input vector of 784 spikes along with 2 neuromodulatory bits. It is composed of 100 fully connected SRC neurons. The input current of each SRC is computed following the equation

$$I[t] = \beta I[t - 1] + \sum_{i=0}^n W_i Input_i \quad (4)$$

where $n = 783$ in our experiments. The weight matrix W_{ij} is imported into the FPGA using a Julia script that generates a file named “WeightMatrix01_pkg.vhd”, which can be directly used in VHDL. In order to analyze the effect of quantization, the script adjusts the weight bit-width from 9 down to 2 bits (including the sign bit). No additional processing is applied to the weight matrices, in order to validate the robustness of the SRC model. The corresponding results are presented in the following section.

The IR layer receives as input a vector of 100 spikes generated by the SRC layer. The ten IR neurons are fully connected and perform the summation of their inputs as described in equation 5.

$$S_{out}[t] = S_{out}[t - 1] + \sum_{i=1}^n Input(i) * k(i), \quad (5)$$

Since all weights in the IR weight matrix take values of either -1 or $+10$, and in order to limit memory usage, the value -1 is encoded as ‘0’ and the value $+10$ as ‘1’. A subsequent `if` statement is then used to restore the original values. This reduces each IR weight to a single bit. A Julia script exports this matrix into the file “WeightMatrix02_pkg.vhd”, which is directly usable in VHDL.

The SRC and IR weight matrices are stored in LUT-registers. This choice provides faster access than BRAM, which typically requires at least one clock cycle. This is made possible by the moderate size of the network and the large number of LUTs available on the XC7A200T device.

4.3 Output layer

This layer is used for analysis purposes. It takes as input the 10 IR output values and provides the index of the maximum value. At the end of a spiking trace, this index is compared with `CMP_VAL` through the activation of the μ -`CMP` signal. In case of a mismatch, an error counter is incremented and subsequently used to compute the recognition accuracy.

4.4 Display unit - HUB75

A display unit is implemented to visualize the network behavior during the debugging phase. It uses a 32×64 LED matrix with a HUB75 interface. The image sequence of a spiking trace is displayed on the right side, while the recognized digit is displayed on the left side as shown Figure 6.

5 Experimental results

Figure 10 shows the experimental setup used to validate and analyze SRC network performance. All tests were performed on an Alinx board equipped with an AMD Xilinx Artix-7 XC7A200T. All the results presented in this section are obtained using the MNIST dataset, converted into Spiking Traces as described previously.

We first validate the behavior of the VHDL implementation by comparing it with the PsV version coded in Julia. The entire SpT test set is processed on both systems. The parameters z_s^{hyp} and z_s^{deep} are set to 900 and 100, respectively, in both cases. The SRC input weight matrices are encoded using 9 bits (from -256 to $+255$). The VHDL implementation deployed on the FPGA achieves an accuracy of 96.31%, which is identical to that of the PsV implementation in Julia (96.31%).

We then analyze the computation time and the hardware resource utilization of the FPGA. The computation time directly influences the energy consumed to process each digit. A digit corresponds to a spiking trace of 220 images. The SRC layer is the slowest layer of the network: each SRC neuron requires 784 clock cycles to process a single image. At the end of each image processing step, 8 additional clock cycles are required for buffering and for resetting the state machines. This results in a total of 174,240 clock cycles per digit. At a clock frequency of 100 MHz, this corresponds to a processing time of 1.7424 ms per digit. The processing time is then reduced by shortening the spiking trace length, and the resulting degradation in accuracy is evaluated. Table 3 shows a significant degradation for sequences shorter than 44 images.

Table 3. Spiking trace length vs. accuracy and energy efficiency at 100 MHz.

size	acc. (%)	T/SpT (ms)	E/SpT (mJ)
20+200	96.31	1.748	2.24
10+100	95.66	0.871	1.11
5+50	95.25	0.436	0.55
4+40	94.17	0.348	0.45
2+20	91.99	0.174	0.22

Table 4. FPGA: resource report per SRC neuron.

Neuron type	LUTs	FFs	BRAM	DSP
SRC (W:9 bits)	830	132	0	100
SRC (W:4 bits)	789	123	0	100
IR	33	48	0	0
Input	1924	1646	341	0

Finally, the energy per digit can be estimated from Vivado power estimation (post-implementation). Vivado reports the power consumption of the implemented logic after compilation. The total reported consumption is 1.28 W (including the HUB75 display). The last column of Table 3 provides the energy required to process a single digit, expressed in mJ. To avoid an excessive degradation of accuracy, the following tests are not conducted using sequences shorter than 44 images.

Reducing hardware resource utilization can also contribute to lowering energy consumption. Vivado provides a breakdown in terms of LUTs, FFs, BRAMs, and DSPs. This decomposition is reported in Table 4. It is possible to reduce the number of LUTs used per SRC neuron by decreasing the bit-width of the input weight registers. Table 4 highlights a gain of approximately 5 to 6% when moving from 9-bit to 4-bit weights.

5.1 Binary quantization

Table 5 presents the results obtained by varying the register size of the SRC weight matrix. The maximum size is 9 bits, and the minimum size is 2 bits (including the sign bit). A significant degradation is observed when the weight register size is less than or equal to 3 bits. In contrast, the use of 4-bit weights represents an attractive trade-off: accuracy remains acceptable while LUT utilization is reduced by approximately 5 to 6% (Table 4), which should lead to a proportional reduction in power consumption due to the released logic resources. The results also show that the spike generation rate can be reduced by increasing z_s^{hyp} (Figure 5).

The reference value of z_s^{hyp} is set to 900 in order to closely match the behavior reported by De Geeter et al. [6]. However, higher values (e.g., 980) significantly reduce spiking activity (by approximately a factor of ~ 3 between 880 and 980 in our observations). This suggests that an *event-based* implementation could become advantageous when activity is sufficiently sparse.

We then analyze recognition accuracy when weight quantization is combined with a reduction in spiking trace length, for z_s^{hyp} values ranging from 880 to 980. The results are reported in Table 6. When spiking trace length becomes smaller and weights are quantized on 4 bits, we start to see a decrease in accuracy for low spiking frequencies (i.e. higher z_s^{hyp} values).

Table 5. Weight bit-width vs. accuracy for different values of z_s^{hyp} .

size	acc. (%) $z_s^{hyp}=880$	acc. (%) $z_s^{hyp}=900$	acc. (%) $z_s^{hyp}=920$	acc. (%) $z_s^{hyp}=940$	acc. (%) $z_s^{hyp}=960$	acc. (%) $z_s^{hyp}=980$	acc. (%) $z_s^{hyp}=1000$
9	96.13	96.31	96.26	96.28	96.02	95.58	93.23
8	96.17	96.25	96.21	96.31	96.07	95.45	92.98
7	96.06	96.27	96.21	96.30	96.07	95.52	92.72
6	96.15	96.26	96.26	96.24	95.88	95.22	92.18
5	96.04	96.14	96.35	96.13	95.73	94.43	90.64
4	95.17	95.35	95.40	95.36	93.75	91.60	86.17
3	90.72	91.01	90.69	89.94	86.00	81.37	73.16
2	55.01	54.82	53.74	51.48	47.61	43.67	37.58

Table 6. SpT vs Size Reg. vs z_s^{hyp}

Size SpT	880			900			920		
	6 bits	5 bits	4 bits	6 bits	5 bits	4 bits	6 bits	5 bits	4 bits
55	95.13%	95.05%	94.38%	93.81%	93.32%	91.90%	94.26%	93.68%	92.48%
44	94.07%	93.66%	92.39%	94.39%	93.91%	92.89%	94.87%	94.34%	93.44%
Size SpT	940			960			980		
	6 bits	5 bits	4 bits	6 bits	5 bits	4 bits	6 bits	5 bits	4 bits
55	94.78%	94.17%	92.99%	90.24%	89.02%	85.35%	90.74%	89.97%	86.46%
44	91.10%	89.78%	87.05%	90.71%	89.49%	86.63%	91.40%	90.72%	88.17%

5.2 Comparison with other SNN FPGA implementations

Our results are compared with other FPGA-based SNN implementations evaluated on the MNIST dataset. To ensure a fair comparison, the operating frequency is normalized to 100 MHz. Since the neuron model proposed in this work (SRC) differs from conventional approaches, the comparison is conducted with studies employing neurons of comparable complexity (LIF and variants) as well as neural networks of similar size.

For comparable weight matrix word widths (4 bits), comparing the accuracy gaps between the training and test datasets across the different works reveals a discrepancy of 3% in the study by Carpegna et al. [4] and more than 70% by Han et al. [9], which is significantly higher than the 1.1% observed in this work. This strong preservation of accuracy after FPGA deployment could be attributed to the robustness of the underlying neuronal model, which implements spiking dynamics without reset through a mixed feedback interconnection.

The processing time per digit is below one millisecond for short spiking traces and is comparable to that reported by Carpegna et al. [4], while the energy consumption is particularly low. This performance is primarily due to (i) extensive operator simplifications, (ii) full parallelization within each layer, and (iii) the use of DSP48 units in SRC computations. As a result, SRC neurons are able to compete with LIF neurons in terms of computation time and energy consumption, while preserving continuous dynamics that are closer to those of biological neuron models, as well as analog electronic implementations [12, 15].

Table 7. Comparison of this SRC implementation with FPGA-based SNNs.

Design	Carpegna et al. [4]	Han et al. [9]	this work (200 - 20)	this work (44 - 4)
Year	2024	2020	2025	2025
Model	LIF	LIF	SRC	SRC
Neurons	784-128-10	784-1024-1024-10	784-100-10	784-100-10
FPGA	XC7Z020	C7Z045 SoC	XC7A200	XC7A200
<i>freq.</i> [MHz]	100	100 ¹	100	100
Cells log.	7,612	12,690	-	93,347
DSP used	0	-	100	100
BRAM used	18	40.5	341 ²	341 ²
<i>T/img</i> [ms]	0.78	12.42 ¹	1.748	0.436
<i>E/img</i> [mJ]	0.14	5.92 ¹	2.24	0.55
Training accur. [%]	96.83	98.48	96.48	96.48
Weight (bits)	4	6 (4)	4	4
FPGA accur. [%]	93.85	97.06 (<20)	95.35	92.89

¹ adjust from 150 to 100 MHz

² BRAM is used for storing the spiking traces.

6 Discussion

The experiments highlight two main trade-offs. First, reducing the length of the spiking traces linearly decreases the processing time and energy consumption, but the accuracy degrades when the sequence length falls below approximately 44 images (Table 3). Second, weight quantization reduces the usage of logic resources (and thus potentially the power consumption), but the accuracy degrades sharply when the word width is reduced below 4 bits (Table 5). In our configuration, 4 bits therefore appears to be a practical lower bound.

Another important control parameter is z_s^{hyp} , which directly regulates the spike generation frequency (Figure 5). We observe that increasing z_s^{hyp} can reduce spiking activity by a factor of approximately three (from 880 to 980) while maintaining an acceptable level of accuracy. This suggests that an *event-driven* scheduling strategy could become advantageous when the spiking activity is sufficiently sparse. A natural extension of this work is therefore to investigate a hybrid approach capable of switching between synchronous processing and *event-driven* execution depending on the observed spike density.

Finally, beyond reporting energy consumption per digit or per image, it may be more informative to normalize energy with respect to the number of emitted spikes. A metric such as E/spike could facilitate comparisons between implementations of different sizes and operating frequencies. This would require measuring the total number of spikes produced (e.g., at the SRC outputs and/or across the network layers) and reporting E/spike in addition to E/digit .

7 Conclusion

In this work, we implemented an SRC-based spiking neural network (SNN) on an FPGA accelerator and evaluated it on an Artix-7 XC7A200T FPGA using spiking traces derived from the MNIST dataset. The SRC neuron preserves continuous dynamics while remaining compatible with efficient hardware simplifications in VHDL. Our prototype achieves 96.31% accuracy with a 220-image spiking

trace and a processing time of 1.7424 ms per digit at 100 MHz. We further show that reducing the spiking trace length and quantizing the synaptic weights can significantly lower energy consumption, achieving 93.32% accuracy at 0.55 mJ per digit (55 images, 5-bit weights) and 92.89% at 0.45 mJ (44 images, 4-bit weights). These results indicate that SRC neurons are strong candidates for energy-efficient SNN accelerators. The Binder–NetWorkLevelxx architecture additionally provides high modularity and simplified reconfiguration. Future work includes completing the combined exploration of spiking trace length and weight quantization, investigating adaptive *event-driven* scheduling enabled by reduced spiking activity, and developing automation tools for code generation and interconnection to support larger and potentially multi-FPGA networks.

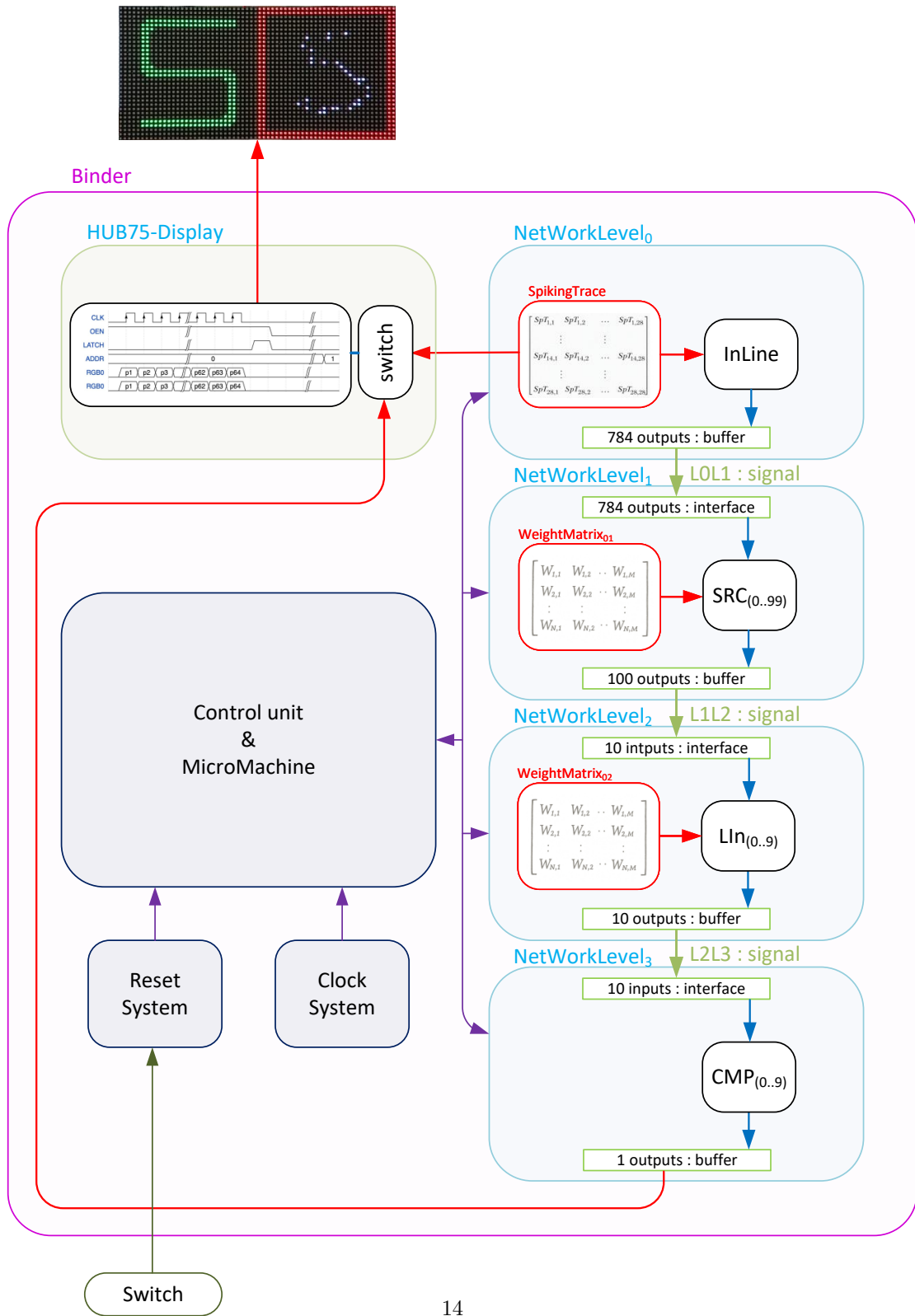


Figure 6. Architecture of the neural network on FPGA.

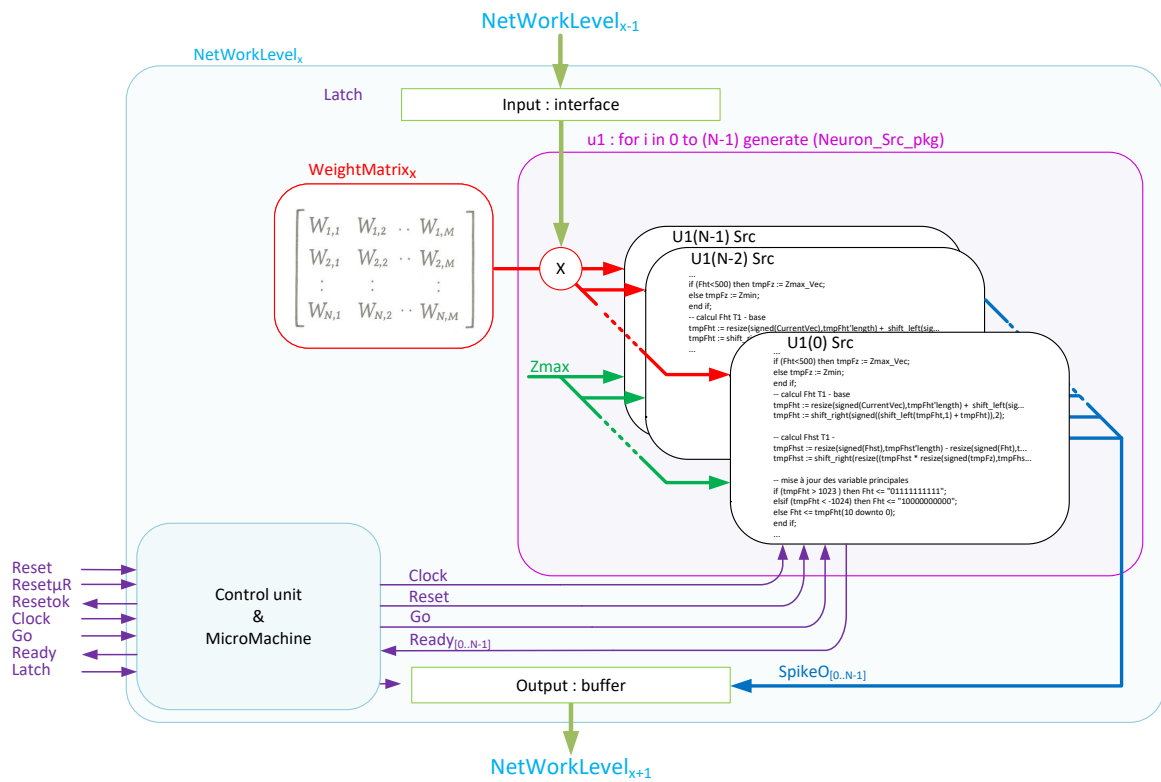


Figure 7. Internal structure of a neural network layer.

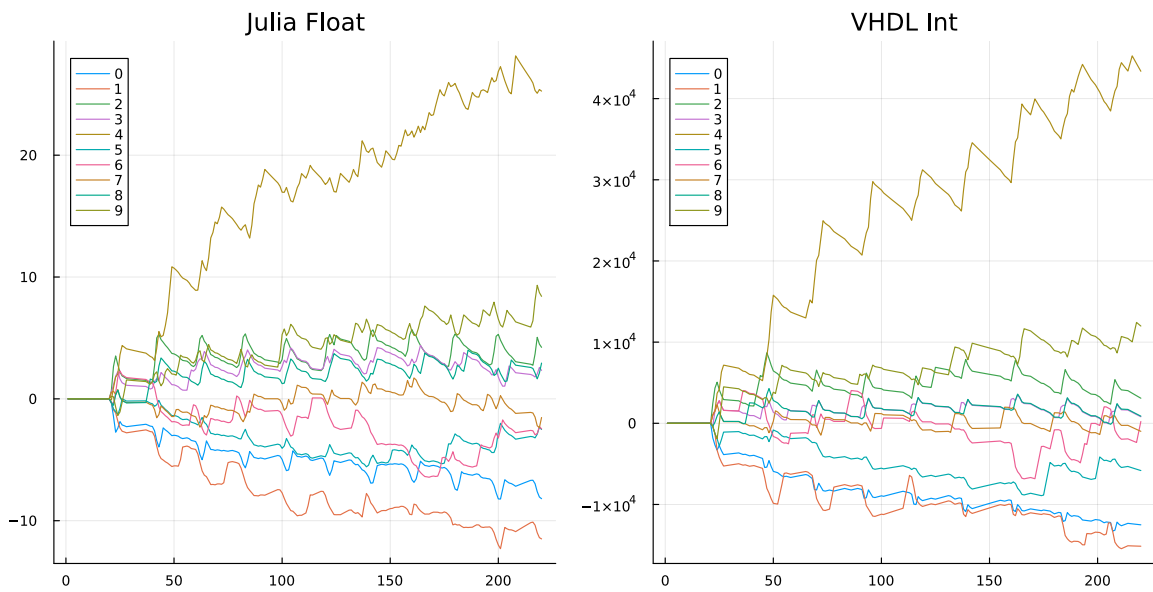


Figure 8. Stability results and accuracy (the two true solutions).

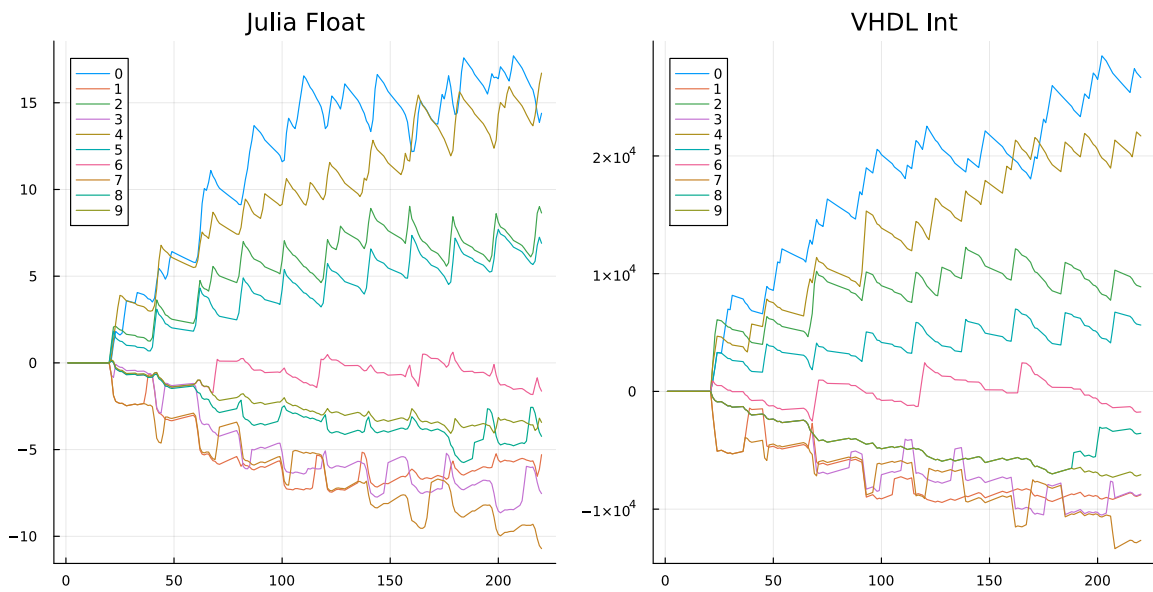


Figure 9. Stability results and accuracy (one true - one false solution).

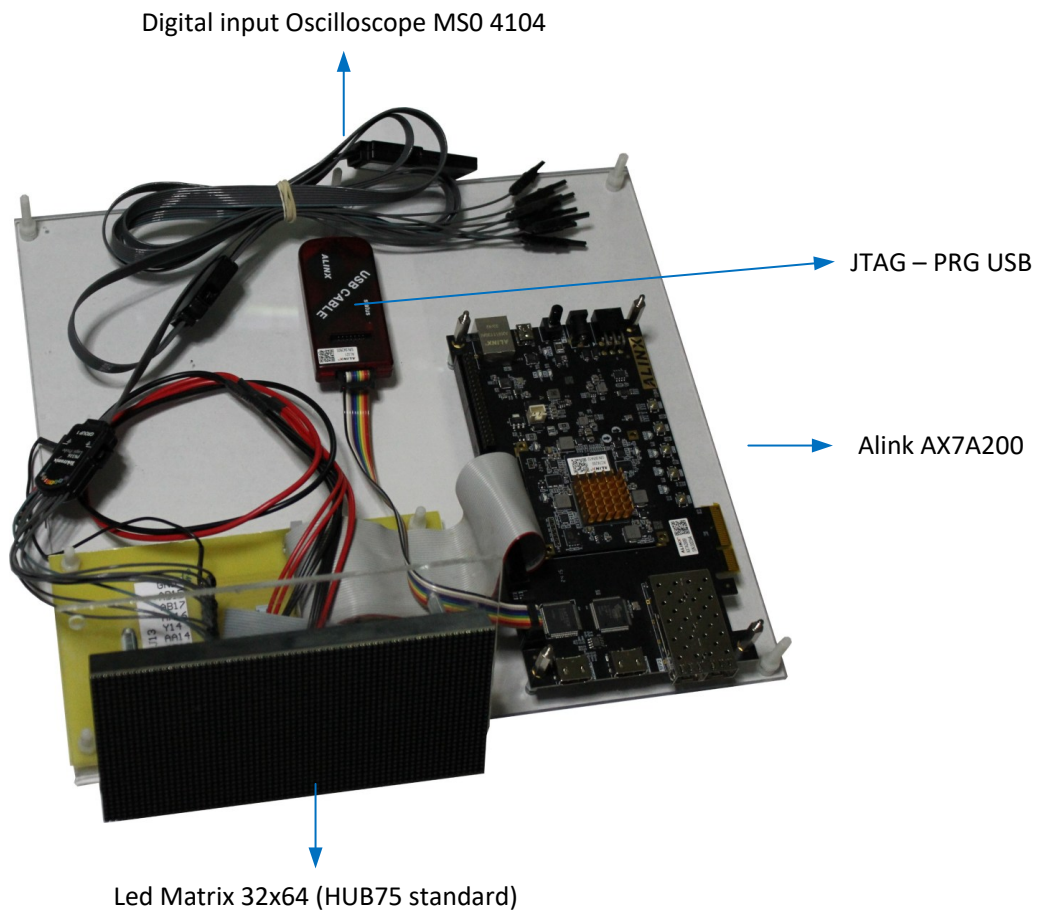


Figure 10. Test setup using the Alinx XC7A200 board.

References

- [1] Larry F Abbott. Lapicque’s introduction of the integrate-and-fire model neuron (1907). *Brain research bulletin*, 50(5-6):303–304, 1999.
- [2] Ilkin Aliyev, Jesus Lopez, and Tosiron Adegbiya. Exploring the sparsity-quantization interplay on a novel hybrid snn event-driven architecture. In *2025 Design, Automation & Test in Europe Conference (DATE)*, pages 1–7. IEEE, 2025.
- [3] Alessio Carpegna, Alessandro Savino, and Stefano Di Carlo. Spiker: an fpga-optimized hardware accelerator for spiking neural networks. In *2022 IEEE Computer Society Annual Symposium on VLSI (ISVLSI)*, pages 14–19. IEEE, 2022.
- [4] Alessio Carpegna, Alessandro Savino, and Stefano Di Carlo. Spiker+: a framework for the generation of efficient spiking neural networks fpga accelerators for inference at the edge. *IEEE Transactions on Emerging Topics in Computing*, 2024.
- [5] Manon Dampfhofer, Thomas Mesquida, Alexandre Valentian, and Lorena Anghel. Are snns really more energy-efficient than anns? an in-depth hardware-aware study. *IEEE Transactions on Emerging Topics in Computational Intelligence*, 7(3):731–741, 2022.
- [6] Florent De Geeter, Damien Ernst, and Guillaume Drion. Spike-based computation using classical recurrent neural networks. *Neuromorphic Computing and Engineering*, 4(2):024007, 2024.
- [7] Jianfeng Feng. Is the integrate-and-fire model good enough?—a review. *Neural networks*, 14(6-7):955–975, 2001.
- [8] Shikhar Gupta, Arpan Vyas, and Gaurav Trivedi. Fpga implementation of simplified spiking neural network. In *2020 27th IEEE International Conference on Electronics, Circuits and Systems (ICECS)*, pages 1–4. IEEE, 2020.
- [9] Jianhui Han, Zhaolin Li, Weimin Zheng, and Youhui Zhang. Hardware implementation of spiking neural networks on fpga. *Tsinghua Science and Technology*, 25(4):479–486, 2020.
- [10] Zhen He, Cong Shi, Tengxiao Wang, Ying Wang, Min Tian, Xichuan Zhou, Ping Li, Liyuan Liu, Nanjian Wu, and Gang Luo. A low-cost fpga implementation of spiking extreme learning machine with on-chip reward-modulated stdp learning. *IEEE Transactions on Circuits and Systems II: Express Briefs*, 69(3):1657–1661, 2021.
- [11] Alan L Hodgkin and Andrew F Huxley. A quantitative description of membrane current and its application to conduction and excitation in nerve. *The Journal of physiology*, 117(4):500, 1952.
- [12] Giacomo Indiveri. Neuromorphic is dead. long live neuromorphic. *Neuron*, 113(20):3311–3314, 2025.
- [13] Jindong Li, Guobin Shen, Dongcheng Zhao, Qian Zhang, and Yi Zeng. Firefly: A high-throughput hardware accelerator for spiking neural networks with efficient dsp and memory optimization. *IEEE Transactions on Very Large Scale Integration (VLSI) Systems*, 31(8):1178–1191, 2023.
- [14] Sixu Li, Zhaomin Zhang, Ruixin Mao, Jianbiao Xiao, Liang Chang, and Jun Zhou. A fast and energy-efficient snn processor with adaptive clock/event-driven computation scheme and online learning. *IEEE Transactions on Circuits and Systems I: Regular Papers*, 68(4):1543–1552, 2021.

- [15] Loris Mendolia, Chenxi Wen, Elisabetta Chicca, Giacomo Indiveri, Rodolphe Sepulchre, Jean-Michel Redouté, and Alessio Franci. A neuromodulable current-mode silicon neuron for robust and adaptive neuromorphic systems. *arXiv preprint arXiv:2512.01133*, 2025.
- [16] Farhad Modaresi, Matthew Guthaus, and Jason K Eshraghian. Openspike: an openram snn accelerator. In *2023 IEEE International Symposium on Circuits and Systems (ISCAS)*, pages 1–5. IEEE, 2023.
- [17] Sathish Panchapakesan, Zhenman Fang, and Jian Li. Syncnn: Evaluating and accelerating spiking neural networks on fpgas. *ACM Transactions on Reconfigurable Technology and Systems*, 15(4):1–27, 2022.
- [18] Arnab Roy, Swagath Venkataramani, Neel Gala, Sanchari Sen, Kamakoti Veezhinathan, and Anand Raghunathan. A programmable event-driven architecture for evaluating spiking neural networks. In *2017 IEEE/ACM International Symposium on Low Power Electronics and Design (ISLPED)*, pages 1–6. IEEE, 2017.
- [19] Frances K Skinner. Conductance-based models. *Scholarpedia*, 1(11):1408, 2006.
- [20] Emma Strubell, Ananya Ganesh, and Andrew McCallum. Energy and policy considerations for deep learning in nlp. In *Proceedings of the 57th annual meeting of the association for computational linguistics*, pages 3645–3650, 2019.
- [21] Qian Wang, Youjie Li, Botang Shao, Siddhartha Dey, and Peng Li. Energy efficient parallel neuromorphic architectures with approximate arithmetic on fpga. *Neurocomputing*, 221:146–158, 2017.
- [22] Jiadong Wu, Lun Lu, Yinan Wang, Zhiwei Li, Changlin Chen, Qingjiang Li, and Kairang Chen. Efficient spiking convolutional neural networks accelerator with multi-structure compatibility. *Frontiers in Neuroscience*, 19:1662886, 2025.
- [23] Zhanglu Yan, Zhenyu Bai, and Weng-Fai Wong. Reconsidering the energy efficiency of spiking neural networks. *arXiv preprint arXiv:2409.08290*, 2024.